Available online at www.sciencedirect.com

ScienceDirect

Ceramics International 40 (2014) 4019–4024

CERAMICS INTERNATIONAL

www.elsevier.com/locate/ceramint

# The preparation, characterization and photocatalytic activity of radical-shaped $CeO_2$/ZnO microstructures

I-Tsan Liu[a], Min-Hsiung Hon[a], Lay Gaik Teoh[b,*]

[a]Department of Materials Science and Engineering, National Cheng Kung University, Tainan 701, Taiwan
[b]Department of Mechanical Engineering, National Pingtung University of Science and Technology, Neipu, Pingtung 912, Taiwan

Received 27 January 2013; received in revised form 24 July 2013; accepted 10 August 2013
Available online 16 August 2013

**Abstract**

This paper uses a wet-chemical precipitation route to prepare radical-shaped ZnO microprisms and to deposit Cerium oxide ($CeO_2$) on the surface of ZnO, to form $CeO_2$/ZnO microstructures. The samples are characterized using X-ray powder diffraction (XRD), scanning electron microscopy (SEM) and UV–vis diffuse reflectance spectroscopy. Their catalytic activity is also evaluated using methylene blue (MB) as a detection reagent. $CeO_2$/ZnO systems exhibit higher UV absorption and transparency in the visible region. The experimental results show that the deposition of $CeO_2$ nanospecies is successful and that the radical-shaped microstructures of ZnO are well maintained. The $CeO_2$/ZnO microstructures exhibit a much greater intensity of UV-light absorptivity and much higher photocatalytic activity than those of radical-shaped ZnO microprisms.


*Keywords:* Radical-shaped ZnO microprisms; Radical-shaped $CeO_2$/ZnO; Methylene blue (MB); UV light absorption; Photocatalytic activity

## 1. Introduction

Nanocomposite materials have many special physical and chemical properties [1]. Not only do they have the nature of their constituents, but also they allow more efficient optical or electrical chemical reactions than do other composite materials. ZnO is a wide and direct band gap semiconductor and ZnO materials are used in many fields, because of their high catalytic efficiency, low cost and environmental sustainability. However, the reactivity of the ZnO surface depends significantly on the particle morphology [2,3]. Therefore, by controlling the ZnO particle morphology, it should be possible to develop a ZnO photocatalyst with high activity. However, ZnO particle morphologies are complex and diversified. ZnO particles with well-defined morphological characteristics, spherical, needle-like, prismatic and rod-like shapes, have been produced [4,5]. The preparation of ZnO aggregates that have a regular shape, such as intertwined ellipsoidal aggregates and flower- and tetrapod-like aggregates, has also been described [6].

$CeO_2$ is one of the most reactive rare earth metal oxides and it has a broad range of applications in various fields, because of its many special properties, such as its high refractive index, high optical transparency in the visible region and its high capacity to store oxygen and insert/extract charge density [7,8]. $CeO_2$/ZnO composites exhibit a unique ability to absorb UV, high stability at high temperatures, good hardness values and low activity as catalysts [9]. Different chemical methods are used for the synthesis of $CeO_2$/ZnO composites, such as atmospheric pressure metal-organic chemical vapor deposition (AP-MOCVD) [10], hydrothermal synthesis [11], the soft solution chemical route [12], the solid-stabilized emulsion route [13], the sol–gel method [14] and the precipitation technique [15]. The precipitation method has several advantages, in that it is simple, cost-efficient, allows the fabrication of products on a large industrial scale and it provides reproducible results. However, most of these procedures involve the precipitation of $Ce^{4+}$ and $Zn^{2+}$ ions and it is difficult to disperse Cerium species on the surface of ZnO to allow more active sites with smaller doses of Cerium. Its tendency to agglomerate into larger particles results in a reduction in their activity during the cycle of use.

This study uses a modified precipitation route, which has two steps, to prepare radical-shaped ZnO microprisms. $CeO_2$ is

*Corresponding author. Tel.: +886 87703202x7527.
*E-mail address:* n5888107@mail.npust.edu.tw (L.G. Teoh).

0272-8842/$ - see front matter © 2013 Elsevier Ltd and Techna Group S.r.l. All rights reserved.
http://dx.doi.org/10.1016/j.ceramint.2013.08.053

easily deposited on the surface of ZnO to form $CeO_2$/ZnO microstructures. The $CeO_2$/ZnO composites are characterized using XRD, SEM and UV–vis diffuse reflectance spectra measurement. Their catalytic and photocatalytic activities are also evaluated and compared with those of pure $CeO_2$ and pure ZnO samples.

## 2. Experimental procedure

For the synthesis of radical-shaped ZnO prisms, (0.01 M) $Zn(NO_3)_2.6H_2O$ and 1.5 ml ethylenediamine were dissolved in 100 ml of de-ionized water. Then, 10 g of hexamethylenetetramine (HMT) was added, while the mixture was stirred. The solution was then aged in a capped flask, at 90 °C for 24 h. The resulting precipitates were collected and washed, using de-ionized water and ethanol. All chemicals were of analytical grade. For the preparation of $CeO_2$/ZnO composite, the as-obtained ZnO product was dispersed in 250 ml of de-ionized water. (0.1 M) $Ce(NO_3)_3.6H_2O$, together with different reverse molar ratios (Ce/Zn)(100/0, 90/10, 50/50, 10/90, 0/100% v/v), was stirred for 2 h, after which 0.5 g poly-(vinyl pyrrolidone) (PVP) was added. The mixture was then stirred quickly for 2 h. The mixture was aged in a capped flask at 70 °C for 5 h. The resulting precipitates were collected and washed, using de-ionized water and ethanol. White powders of the $CeO_2$/ZnO components were obtained at the end of the experimental procedure.

The crystalline structure of the pure and component samples was identified using X-ray diffraction (XRD, Rigaku, Tokyo, Japan), in order to analyze and confirm the crystalline phase structure. The X-ray diffraction used CuKα radiation ($\lambda = 1.54178$ Å) and a Ni filter and operated at 30 kV, 20 mA, with a diffraction range of $2\theta = 25$–75° and a scanning speed of 2 °/min. The microstructure and morphology of the $CeO_2$/ZnO components and catalysts were characterized using scanning electron microscopy (SEM, JEOL JSM-6500FE). The absorption spectra of the samples were recorded using a (JASCO V-760 ultraviolet–visible) spectrophotometer in the range 250–800 nm. The diffuse reflectance spectra are directly measured by the JASCO instrument. The samples were dispersed in ethanol at a concentration of 10 mg/100 ml. In order to ensure that the $CeO_2$/ZnO composite was well dispersed and to guarantee the homogeneity of the final solution, an ultrasonic pool was used to vibrate the mixture for approximately 60 min, before the absorption spectra analysis. Photocatalytic degradation experiments using methylene blue (MB) (10 mg/1000 ml) were performed using a photoreactor, under UV-light irradiation. The light source for the photocatalysis was a mercury (Hg) tube lamp (Philips 18 W, $\lambda < 365$ nm). The volume of the initial MB solution was 100 ml. All powder concentrations in the MB aqueous solution were 10 mg/100 ml. The mixture was stirred in dark for 90 min, in order to ensure absorption/desorption equilibrium at room temperature before photoreaction. The suspension was then stirred magnetically, during irradiation. At regular intervals, samples were withdrawn and centrifuged, to separate solid particles for analysis. The concentration of aqueous MB was determined using a UV–vis spectrophotometer at 663 nm, by measuring its absorbance. The degradation rate was calculated as $(A_0 - A)/A_0 = (C_0 - C)/C_0$ [16], where $A_0$ is the initial maximum absorbance, $A$ is the absorbance after irradiation for a time, $t$, of maximum absorbance, $C$ is the concentration of MB at that time and $C_0$ is the concentration in the adsorption equilibrium, before irradiation. The photoactivity for MB in the presence of pure $CeO_2$ and pure ZnO, under UV-light irradiation, was also evaluated.

## 3. Results and discussion

X-ray diffraction (XRD) is usually used for the identification of crystal phase and the estimation of the crystallite size of each phase. Fig. 1 shows the XRD patterns for the different reverse molar ratios ($CeO_2$/ZnO) (100%/0%, 90%/10%, 50%/50%, 10%/90%, 0%/100% v/v) of the composites, after being calcined at 550 °C for 2 h, which gives a good insight into the crystallinity of the products. It is seen that there are two sets of diffraction peaks for the $CeO_2$/ZnO sample, which indicates that the as-synthesized samples are composite materials. The XRD peaks at $2\theta = 28.54°$, 33.07°, 47.47°, 56.33°, 59.07° and 69.40° are attributable to $CeO_2$, as shown in Fig. 1a. The pure $CeO_2$ has peaks of a weaker intensity than $CeO_2$90%/ZnO peaks (Fig. 1b). The diffraction lines also show a large narrowing of the peaks. This observation indicates that pure $CeO_2$ has crystallites of a larger than average size. Its lattice constant is $a = 5.412$ Å, so it belongs to the space group Fm-3m [225], while the characteristic peaks of the cubic phase $CeO_2$ gradually increase with as the $CeO_2$ content increases, as shown in Fig. 1c and d. These diffraction peaks are identified as that of pure $CeO_2$ with a cubic phase, which is consistent with JCPDS, No. 81-0792. The ZnO phase is clearly observed when the amount of ZnO is increased, while the intensity of $CeO_2$ decreases, correspondingly. The XRD peaks at $2\theta = 31.74°$, 34.38°, 36.01°, 47.48°, 56.54°, 62.78°, 66.30°, 67.87° and 69.01° are attributable to ZnO, as shown in Fig. 1e. Three peaks

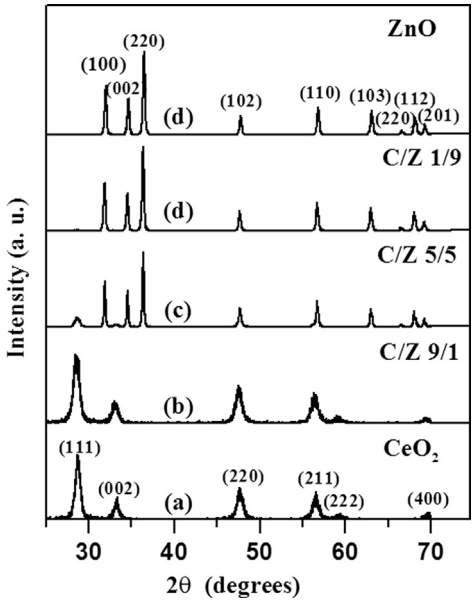


Fig. 1. The XRD patterns for (a) pure $CeO_2$, (b) $CeO_2$90%/ZnO, (c) $CeO_2$50%/ZnO, (d) $CeO_2$10%/ZnO and (e) pure ZnO, after calcination at 550 °C for 2 h.

are located close to each other: $CeO_2$ at 47.47° (220), 56.33° (311) and 69.40° (400), and ZnO at 47.48° (102), 56.54° (110) and 69.01° (222). Pure ZnO exhibits a hexagonal phase, which is consistent with JCPDS, No. 89-1397. The coupled composites indeed consist of both wurtzite ZnO and cubic phase $CeO_2$, and the characteristic peaks of wurtzite ZnO gradually decrease as the Ce/Zn concentration molar ratio increases (0–100%). This demonstrates the successful preparation of coupled bi-component composites that consist of cubic phase $CeO_2$ and wurtzite ZnO.

The morphology, size and microstructure of the samples are investigated in detail using SEM. The SEM images in Fig. 2 show the morphology of the prepared samples. The synthesis of the precipitation system easily leads to the formation of particle clusters of a spheroidal shape. PVP is used as a dual functional reductant and stabilizer for the synthesis of $CeO_2$ nanoplates in aqueous solutions. $CeO_2$ nanospecies are deposited on the surface of ZnO microprisms, as a result of the large PVP–Cerium interaction [17]. Pure $CeO_2$ sample grains have a diameter from 6 to 8 nm and are spherical, as shown in Fig. 2a. In the samples to which ZnO is added and the amount of $CeO_2$ reduced, the $CeO_2$ crystallite consists of nanoparticles and the $CeO_2$ grain size is approximately 6 nm. Crystalline ZnO is observed on $CeO_2$ (90%)/ZnO components, as shown in Fig. 2b. The enlarged SEM image further reveals that the surface of the ZnO is covered with many nanoscale protuberances of $CeO_2$, which indicates the formation of $CeO_2$/ZnO composites. The SEM image of the as-synthesized $CeO_2$ (10%)/ZnO sample, as shown in Fig. 2c, also shows radical-shaped structures. It has been suggested that prism-shaped ZnO microrods are formed as a result of the differences in the growth rates of various ZnO crystal facets [18]. The enlarged SEM image further reveals that the surface of the ZnO microprisms is coherent, with some nanoscale protuberances of $CeO_2$. The average grain size of the agglomerated $CeO_2$ is approximately 150 nm. Fig. 2d shows a general view of the morphology of the ZnO product over a large area, and shows that the product consists of a large quantity of radical-shaped microstructures. The high-magnification SEM image shows that the radical-shaped ZnO microstructures are composed of prism-like micro-rods. Each prism has a length of 2–4 μm and a thickness of approximately 700 nm. The micro-rod is actually a hexagonal-faceted prism with tapered thin nanotips. The identified $CeO_2$/ZnO microstructures disperse $CeO_2$ more efficiently, so they have a higher photocatalytic activity.

Fig. 3 shows the absorption spectra of the $CeO_2$/ZnO samples synthesized at different concentration molar ratios. These synthesized samples exhibit the same low reflectance in the UV region and high reflectance in the visible region. The absorptive spectra concentration of $CeO_2$ is around 325 nm, as shown in Fig. 3a and b. The synthesized samples exhibit intermediate reflection and present a larger slope for the zinc oxide samples, as shown in Fig. 3c–e. The synthesized samples exhibit high absorption from 325 to 375 nm and the

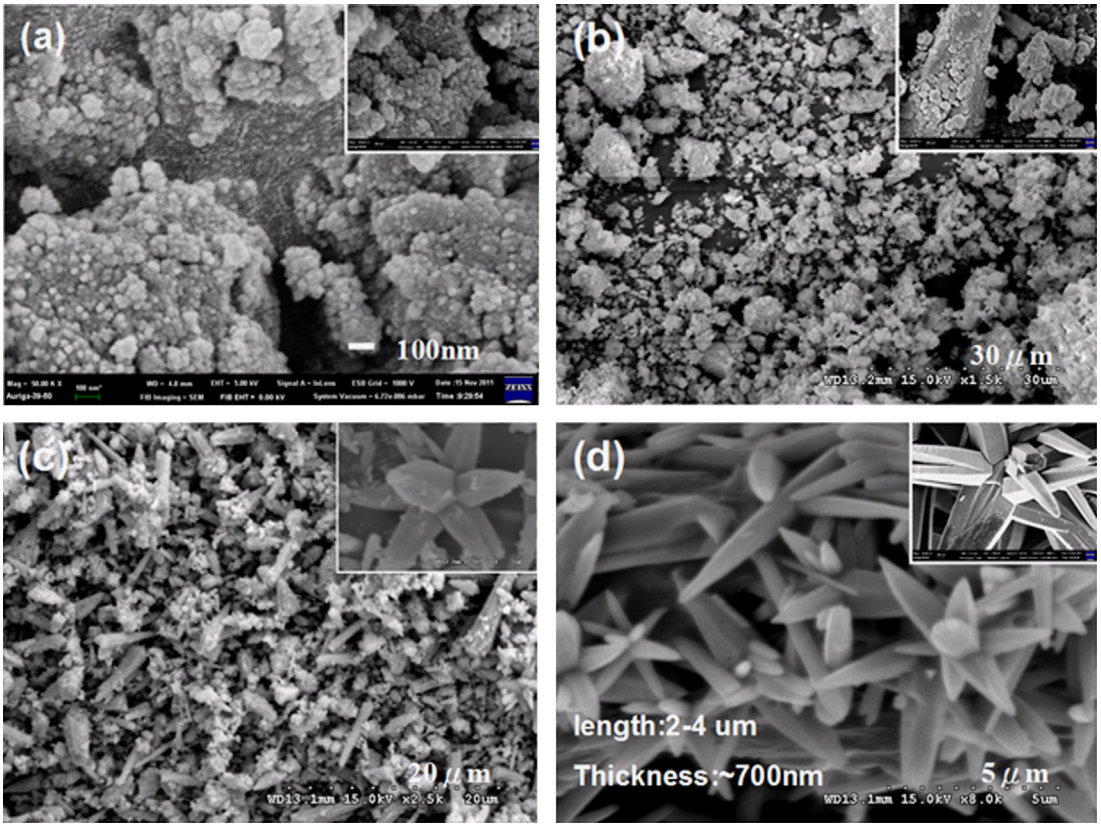


Fig. 2. The SEM images for (a) pure $CeO_2$, (b) $CeO_2$90%/ZnO, (c) $CeO_2$10%/ZnO, and (d) pure ZnO. The inset shows the SEM image for an individual microprism.

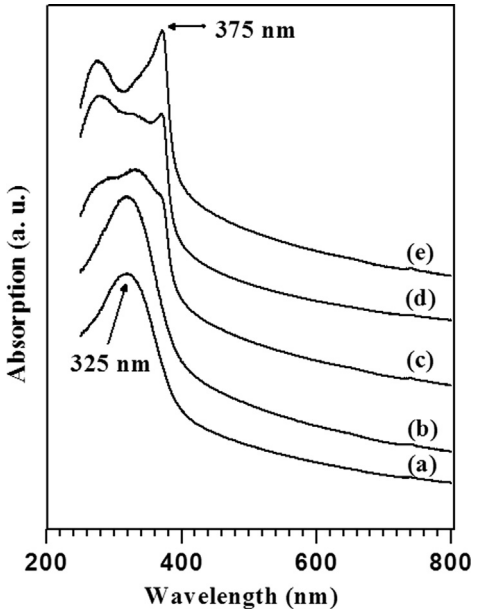


Fig. 3. The UV–vis absorption spectra for (a) pure $CeO_2$, (b) $CeO_2$90%/ZnO, (c) $CeO_2$50%/ZnO, (d) $CeO_2$10%/ZnO and (e) pure ZnO samples calcined at 550 °C for 2 h.

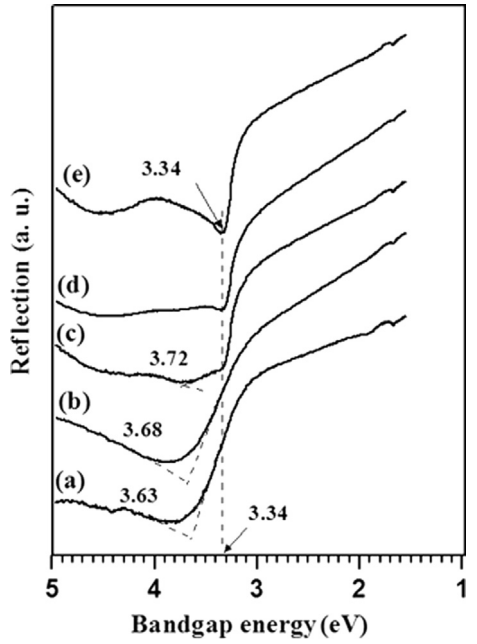


Fig. 4. The UV–vis reflectance spectra for (a) pure $CeO_2$, (b) $CeO_2$90%/ZnO, (c) $CeO_2$50%/ZnO, (d) $CeO_2$10%/ZnO and (e) pure ZnO samples calcined at 550 °C for 2 h.

absorption begins to increase at 375 nm for most of the compounds. However, this behavior is more pronounced in zinc oxide, so the synthesized samples are really promising. When the particle size is reduced, the absorption edge shifts towards a shorter wavelength and there is increased absorption of UV light [19]. A blue-shift phenomenon is seen in many nanomaterials, which can be explained by the quantum confinement effect and the oxygen defects [20].

The UV–vis diffuse reflectance spectra for the band gap energy of the coupled $CeO_2$/ZnO materials are shown in Fig. 4. The band gap value for the samples is calculated using the formula $E_g$ (eV) = 1240/$\lambda_g$ (nm), where $\lambda_g$ is the wavelength value that corresponds to the intersection of the two tangential lines of the spectra. Pure $CeO_2$ has the largest band gap value of 3.63 eV, as shown in Fig. 4a. The band gap energy increases as the $CeO_2$ content decreases, as shown in Fig. 4b (3.68 eV) and Fig. 4c (3.72 eV). For nanomaterials with a particle size down to a few nanometers, the band gap value changes because of the quantum confinement effect. The band gap value is dependent on the particle radius [21]. The change in the optical absorption of binary oxides is mainly due to the decrease in the size of the crystal grain and the interfacial effects between the $CeO_2$ and the ZnO grains. The other samples have a band gap value of 3.34 eV; the value for ZnO is almost the same as the values in Fig. 4d and e. These ZnO crystal grains have a size that is almost in the micro-dimension and their effect can be neglected. The red-shift of the absorption edges and narrowing of the band gaps can account for a large amount of surface defect states, such as Zn interstitials and oxygen vacancies [22]. These defective states seen in the UV–vis diffuse reflectance spectra have an effect on the photocatalytic behavior of the synthesized $CeO_2$/ZnO materials. The synthesized samples exhibit high reflectance from 400 nm, which results in lower absorption in the visible spectrum. Therefore, mixed oxides exhibit high absorption in the UV region (low reflectance) and high transparency in the visible region, which allows their use in sunscreen formulations.

Fig. 5 shows the catalytic absorption/degradation reaction as a function of time for the catalysts. The experiment was conducted without a light source for 90 min, so there was no light irradiation of the $CeO_2$/ZnO samples. It is seen that $CeO_2$ exhibits a higher degradation with MO (methylene orange) than the other samples and it shows the highest absorption/degradation reaction. The degradation rate of MO for the catalyst, shown in Fig. 5a, b, c, d and e, is about 70.8%, 34.6%, 5.6%, 5.2% and 4.9%, respectively. However, the degradation rates of MO are unchanged after 60 min and the degradation rate of MO in the remaining time decreases as the $CeO_2$ components increase. Pure $CeO_2$ has the maximum absorption/degradation reaction, which is the relative value under the same conditions (concentration and amount of catalyst), so the value is not constant, because the ability to decolorize depends mainly on oxygen content and the specific surface area of contact surface. $CeO_2$ is an oxygen-rich material, so it has a strong redox reaction ability. Catalytic efficiency is determined by the concentration of the solution and the ability of the catalyst to release oxygen.

The other experiment with the $CeO_2$/ZnO samples involves irradiation. The results of these experiments are shown in Fig. 6. The rate of degradation of MB for the different molar ratios of $CeO_2$/ZnO ((a) 100%/0%, (b) 90%/10%, (c) 50%/50%, (d) 10%/90% and (e) 0%/100%) as photocatalysts is 2.3%, 7.4%, 28.8%, 67.4% and 52.3%, respectively. The highest photocatalytic activity is for $CeO_2$10%/ZnO (67.4%), and the lowest is for pure $CeO_2$ (2.3%). The photocatalytic activity increases as the ZnO component increases, but the photocatalytic activity for

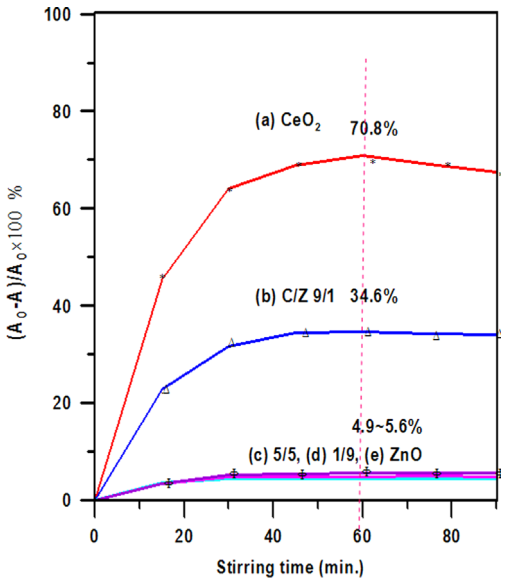


Fig. 5. The degradation of methylene orange using (a) pure $CeO_2$, (b) $CeO_2$90%/ZnO, (c) $CeO_2$50%/ZnO, (d) $CeO_2$10%/ZnO and (e) pure ZnO samples in dark, after stirring for 90 min.

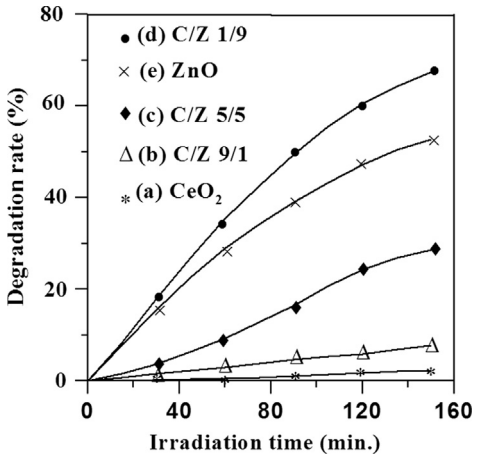


Fig. 6. The Photocatalytic degradation of methylene blue using (a) pure $CeO_2$, (b) $CeO_2$90%/ZnO, (c) $CeO_2$50%/ZnO, (d) $CeO_2$10%/ZnO and (e) pure ZnO samples under irradiation by UV light for 150 min.

$CeO_2$10%/ZnO is higher than for pure ZnO. Furthermore, the notable red-shift in the absorption edge allows the bi-component oxides to better utilize UV light, which also contributes to the high photocatalytic activity. The higher photocatalytic activity of the hierarchical $CeO_2$/ZnO materials can also be attributed to the redox couple, $Ce^{3+}/Ce^{4+}$, the higher capacity to store oxygen [23] and the higher special surface area. After UV irradiation, $CeO_2$ generates electron–hole pairs. Holes produce oxygen molecules or OH radicals (radical), with strong oxidizing ability. Electron in the presence of oxygen generate hydrogen peroxide $H_2O_2$ or superoxide molecules (super oxygen, $O^{2-}$). This shows that $CeO_2$ is less likely to generate electron–hole pairs under the same UV irradiation conditions. A $CeO_2$ catalyst has a strong catalytic activity and a low photocatalytic activity.

## 4. Conclusions

Radical-shaped ZnO microprisms and $CeO_2$/ZnO microstructures are successfully prepared via a simple solution route. The ZnO microstructure is coherent, with some nanoscale protuberances of $CeO_2$. The average grain size of the $CeO_2$ is approximately 6 nm. Each prism has a length of 2–4 μm and a thickness of approximately 700 nm. The micro-rod is actually a hexagonal-faceted prism with tapered thin nanotips. The morphological reformation of ZnO particles results in an enhancement of the highly active face that is exposed to the surface. Using the $CeO_2$/ZnO microstructures as the catalysts for MB, the degradation of MB corresponds with that for the use of $CeO_2$/ZnO nanoparticles, while the $CeO_2$/ZnO nanostructure microprisms have a much longer operating life, because of their size and morphological stability. It is expected that these nanostructure microprisms will have applications in other catalytic reactions.

## References

[1] A.P. Alivisatos, Semiconductor clusters, nanocrystals, and quantum dots, Science 271 (1996) 933–937.
[2] D. Li, H. Haneda, Morphologies of zinc oxide particles and their effects on photocatalysis, Chemosphere 51 (2003) 129–137.
[3] V. Bolis, B. Fubini, E. Giamello, A. Reller, Effect of form of the surface reactivity of differently prepared zinc oxides, Journal of the Chemical Society, Faraday Transactions 1: Physical Chemistry in Condensed Phases 85 (1989) 855–867.
[4] A. Chittofrati, E. Matijević, Uniform particles of zinc oxide of different morphologies, Colloids and Surfaces 48 (1990) 65–78.
[5] T. Trindade, J.D.P. de Jesus, P. O'Brien, Preparation of zinc oxide and zinc sulfide powders by controlled precipitation from aqueous solution, Journal of Materials Chemistry 4 (1994) 1611–1617.
[6] J. Zhang, L.D. Sun, J.L. Yiu, H.L. Su, C.S. Liao, C.H. Yan, Control of ZnO morphology via a simple solution route, Chemistry of Materials 14 (2002) 4172–4177.
[7] R.G. Toro, G. Malandrino, I.L. Fragalà, R.L. Nigro, M.L.G. Bruno, Relationship between the nanostructures and the optical properties of $CeO_2$ thin films, The Journal of Physical Chemistry B 108 (2004) 16357–16364.
[8] C.O. Avellaneda, M.A.C. Berton, L.O.S. Bulhões, Optical and electrochemical properties of $CeO_2$ thin film prepared by an alkoxide route, Solar Energy Materials and Solar Cells 92 (2008) 240–244.
[9] K. Tennakone, J. Bandara, Photocatalytic activity of dye-sensitized tin (IV) oxide nanocrystalline particles attached to zinc oxide particles: long distance electron transfer via ballistic transport of electrons across nanocrystallites, Applied Catalysis A: General 208 (2001) 335–341.
[10] A.M. Torres-Huerta, M.A. Domínguez-Crespo, S.B. Brachetti-Sibaja, H. Dorantes-Rosales, M.A. Hernández-Pérez, J.A. Lois-Correa, Preparation of ZnO:$CeO_{2-x}$ thin films by AP-MOCVD: structural and optical properties, Journal of Solid State Chemistry 183 (2010) 2205–2217.
[11] T.Y. Ma, Z.Y. Yuan, J.L. Cao, Hydrangea-like meso/macroporous ZnO–$CeO_2$ binary oxide materials: synthesis, photocatalysis and CO oxidation, European Journal of Inorganic Chemistry 5 (2010) 716–724.
[12] R. Li, S. Yabe, M. Yamashita, S. Momose, S. Yoshida, S. Yin, T. Sato, Synthesis and UV-shielding properties of ZnO- and CaO-doped $CeO_2$ via soft solution chemical process, Solid State Ionics 151 (2002) 235–241.
[13] Y. He, X. Yu, T. Li, L. Yan, B. Yang, Preparation of $CeO_2$/ZnO nanostructured microspheres and their catalytic properties, Powder Technology 166 (2006) 72–76.
[14] J.F. de Lima, R.F. Martins, C.R. Neri, O.A. Serra, ZnO:$CeO_2$-based nanopowders with low catalytic activity as UV absorbers, Applied Surface Science 255 (2009) 9006–9009.

[15] L.Y. Mo, X.M. Zheng, C.T. Yeh, A novel $CeO_2$/ZnO catalyst for hydrogen production from the partial oxidation of methanol, ChemPhysChem 6 (2005) 1470–1472.
[16] L.Z. Li, B. Yan, $CeO_2$–$Bi_2O_3$ nanocomposite: two step synthesis, microstructure and photocatalytic activity, Journal of Non-Crystalline Solids 355 (2009) 776–779.
[17] Y. Xiong, I. Washio, J. Chen, H. Cai, Z.Y. Li, Y. Xia, Poly(vinyl pyrrolidone): a dual functional reductant and stabilizer for the Facile synthesis of noble metal nanoplates in aqueous solutions, Langmuir 22 (2006) 8563–8570.
[18] H. Usui, Influence of surfactant micelles on morphology and photoluminescence of zinc oxide nanorods prepared by one-step chemical synthesis in aqueous solution, The Journal of Physical Chemistry C 111 (2007) 9060–9065.
[19] J.I. Pankove, Optical Processes in Semiconductors, Dover Publications, Inc., New York, 1971.
[20] S. Tsunekawa, T. Fukuda, A. Kasuya, Blue shift in ultraviolet absorption spectra of monodisperse $CeO_{2-x}$ nanoparticles, Journal of Applied Physics 87 (2000) 1318–1321.
[21] J. Schoonman, Nanoionics, Solid State Ionics 157 (2003) 319–326.
[22] M.S. Mo, J.C. Yu, L. Zhang, S.K.A. Li, Self-assembly of ZnO nanorods and nanosheets into hollow microhemispheres and microspheres, Advanced Materials 17 (2005) 756–760.
[23] T. Masui, M. Yamamoto, T. Sakata, H. Morib, G.Y. Adachi, Synthesis of BN-coated $CeO_2$ fine powder as a new UV blocking material, Journal of Materials Chemistry 10 (2000) 353–357.